ACS APPLIED MATERIALS & INTERFACES

www.acsami.org

Research Article

Creation of Porous, Perfusable Microtubular Networks for Improved Cell Viability in Volumetric Hydrogels

Christian Buckley, Haoyu Wang, Robert O'Dell, Matthew Del Rosario, Matangi Parimala Chelvi Ratnamani, Mark Rome, and Hongjun Wang*

Cite This: *ACS Appl. Mater. Interfaces* 2024, 16, 18522−18533

Read Online

ACCESS | Metrics & More | Article Recommendations | Supporting Information

ABSTRACT: The creation of large, volumetric tissue-engineered constructs has long been hindered due to the lack of effective vascularization strategies. Recently, 3D printing has emerged as a viable approach to creating vascular structures; however, its application is limited. Here, we present a simple and controllable technique to produce porous, free-standing, perfusable tubular networks from sacrificial templates of polyelectrolyte complex and coatings of salt-containing citrate-based elastomer poly(1,8-octanediol-*co*-citrate) (POC). As demonstrated, fully perfusable and interconnected POC tubular networks with channel diameters ranging from 100 to 400 μm were created. Incorporating NaCl particulates into the POC coating enabled the formation of micropores (~19 μm in diameter) in the tubular wall upon particulate leaching to increase the cross-wall fluid transport. Casting and cross-linking gelatin methacrylate (GelMA) suspended with human osteoblasts over the free-standing porous POC tubular networks led to the fabrication of 3D cell-encapsulated constructs. Compared to the constructs without POC tubular networks, those with either solid or porous wall tubular networks exhibited a significant increase in cell viability and proliferation along with healthy cell morphology, particularly those with porous networks. Taken together, the sacrificial template-assisted approach is effective to fabricate tubular networks with controllable channel diameter and patency, which can be easily incorporated into cell-encapsulated hydrogels or used as tissue-engineering scaffolds to improve cell viability.

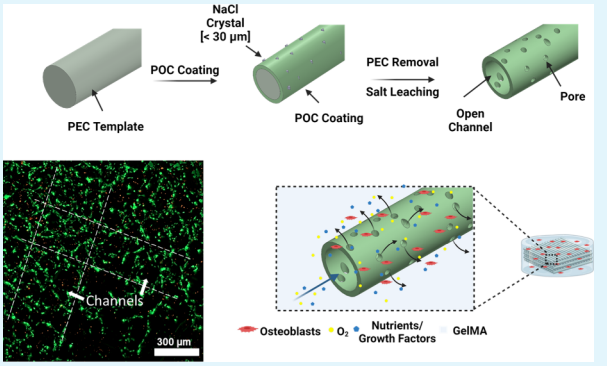

KEYWORDS: *polyelectrolyte complex (PEC), poly(1,8-octanediol-co-citrate), tubular networks, 3D embedded printing, GelMA cell casting*

1. INTRODUCTION

Tissue engineering, an interdisciplinary endeavor with the ultimate goal of regenerating or replacing damaged and diseased tissues,[1] has made astounding progress in various technical fronts, including, but not limited to, the establishment of induced pluripotent stem cells as a robust cell source, insights on the microenvironment-mediated cell phenotype, and spatial control of cell organization via 3D bioprinting.[2−4] However, successful demonstration of its clinical utility remains limited to avascular cartilage or thin dermal/skin equivalents.[5] Although volumetric tissues with structural and compositional complexity are much more desirable for restoring the lost functions of damaged tissues, the noted difficulties of recapitulating the architectural complexity, cellular heterogeneity, and sufficient vascularization have significantly slowed clinical advances.[6] The advent of bioprinting has alleviated some of these challenges by fabricating more intricate scaffolds to better mimic the desired tissue topography and by spatiotemporally populating 3D prints with various cell types.[7] Unfortunately, poor vascularization continues to be a bottleneck for clinically sized, volumetric scaffolds to promote adequate tissue ingrowth with sustained functionality and prolonged viability.[8−10]

Current strategies for introducing vasculature into tissue-engineering scaffolds often rely on the infiltration of host native blood vessels through angiogenesis, typically accomplished through the incorporation of proangiogenic growth factors [e.g., vascular endothelial growth factor (VEGF)].[11−13] This approach, however, is severely limited by the rate of angiogenesis of native blood vessels, which is estimated to be roughly 5 μm/h.[14] As such, a scaffold with dimensions of a few millimeters to centimeters would take weeks to be fully vascularized even under optimal conditions, thereby unavoidably leading to a hypoxic and necrotic core, as well as heterogeneous regions of cell density and phenotype.[15] To

Received: January 13, 2024
Revised: March 19, 2024
Accepted: March 25, 2024
Published: April 2, 2024

https://doi.org/10.1021/acsami.4c00716
ACS Appl. Mater. Interfaces 2024, 16, 18522−18533

address this issue, direct bioprinting and template printing methods have been explored to create vascular-like networks within 3D scaffolds, offering immediate perfusion of nutrients through open channels of a designed architecture.[16,17]

Direct bioprinting, i.e., printing tubular structures with vascular cells (endothelial cells or smooth muscle cells) suspended within the supporting material, offers immediate support for cell growth and matrix production. Gelatin methacrylate (GelMA) or derivatives of polyethylene glycol used to encapsulate endothelial cells for direct printing can support sustained cell viability and continued expression of vascular markers.[18,19] Alternatively, template-based printing normally involves the printing of a sacrificial template that is used to create a channel structure within a cast material upon removal. The templates can be removed manually or through dissolution in an appropriate solvent, leaving an open channel for nutrient perfusion and diffusion into the bulk cast. As demonstrated, cells in a cast construct with perfusable channels indeed show improved cell viability and metabolic activity within the proximity of the channels.[20,21] Despite their demonstrated potential for vitalizing encapsulated cells, both strategies suffer from significant limitations. For example, many hydrogels used in the bioprinting of vascular channels lack the adequate mechanical strength and stability to support loads or tissue growth before channels inevitably collapse from material degradation.[22−24] Inclusion of other materials, such as polymeric fiber fragments, carbon nanotubes, or hydroxyapatite particles into hydrogels, can partially improve the mechanical stability and can be physically blended without involving cytotoxic solvents.[25−29] However, these additives may affect printability, and the degradation byproducts need to be considered for their cytocompatibility. In addition, only a few select materials (e.g., sugar[30]) can be adopted for template-based channel formation without harming cells.[31−34] Solvents used for template dissolution can often damage cells or lead to high localized concentrations of template material byproducts.

Herein, we present a novel and effective strategy to create free-standing, acellular tubular networks that are fully perfusable and can be readily combined with other materials, specifically cell-laden hydrogels. This current work takes advantage of our recently established capability of printing 3D filament structures out of a sacrificial polyelectrolyte complex (PEC), which can be rapidly dissolved in concentrated potassium bromide (KBr) solution.[35] Similarly, 3D filament structures were printed from the PEC ink and then dip-coated with a continuous, thin layer of elastomeric polymer, poly(1,8-octanediol-*co*-citrate) (POC), which led to the formation of free-standing tubular networks upon removal of the PEC template by incubation in KBr solution. POC, commonly used for vascular grafts, was chosen as the coating material due to its unique characteristics, including simple fabrication methods and demonstrated cytocompatibility.[36−38] This work explored the ability to create perfusable tubular networks with varying channel diameters and micropores across the channel wall to promote nutrient diffusion while ultimately sustaining cell viability over an extended period in volumetric cell-laden hydrogels by incorporating such perfusable networks.

2. MATERIALS AND METHODS

2.1. Materials. Poly(diallyldimethylammonium chloride) (PDADMAC, M_W = 200,000−350,000 Da), poly(styrene sulfonic acid) sodium salt (PSS, M_W = 500,000 Da), sodium chloride (NaCl, > 99.0%), pluronic F127, citric acid anhydrous (M_W = 192.1), potassium bromide (KBr, > 99.0%), gelatin from porcine skin (Type A), and methacrylic anhydride were purchased from Sigma-Aldrich (St. Louis, MO). 1,8-Octanediol (98%, MW = 146.23), ethanol (99.5%, ACS reagent grade), methylene blue (M_W = 373.90), lithium phenyl(2,4,6-trimethylbenzoyl) phosphinate (LAP, > 98.0%, M_W = 294.21), penicillin-streptomycin (P/S, 10,000 U/mL), and LIVE/DEAD viability/cytotoxicity kit were purchased from ThermoFisher (Waltham, MA). CellTiter-Glo 3D was purchased from Promega (Madison, WI). Fetal bovine serum (FBS) was obtained from Atlantic Biologicals (Atlanta, GA).

2.2. Cell Culture. Human fetal osteoblasts, hFOB 1.19 (ATCC, Manassas, VA), were cultured in complete growth medium composed of DMEM/F12 (1:1) (Gibco, Grand Island, NY) with 10% FBS and 1% P/S. Cells were maintained at the permissive temperature of 34 °C for proliferation with 5% CO_2 and 95% humidity until reaching roughly 80% confluence prior to subculture.

2.3. Formulation of PEC Ink and 3D Printing of PEC Templates. PEC ink was formulated and prepared as previously described.[35] Briefly, PDADMAC and PSS were separately dissolved in deionized (DI) water with 0.25 M NaCl at a concentration of 2.5 M regarding their monomer units. Solutions were then slowly added in a flask under vigorous stirring at a 1:1 (v/v) ratio and allowed to mix for 30 min. Precipitate was collected in 50 mL centrifuge tubes and centrifuged at 10,000 rpm for 15 min to remove excess water (Sorvall Legend XR1 centrifuge, Thermo Scientific). Collected PEC precipitate was dried overnight at 50 °C and then submerged in excess 1.9 M KBr for 12 h to create a coacervate that would be used as the printable PEC ink.

PEC coacervate was loaded into a 3 mL syringe fitted with a blunt 26G needle and placed on a syringe pump with varying feed rates from 0.1 to 1.2 mL/h. Pluronic F127, dissolved in DI water (25%, w/v) overnight, was transferred to a 35 mm Petri dish to fill half the height of the dish and then left undisturbed at room temperature to solidify. This served as a supporting matrix for the embedded printing of 3D PEC templates with our customized 3D printer. KBr concentration in the PEC ink determines the degree of coacervation, and dilution of KBr through immersion in the DI water in the Pluronic supporting matrix causes the PEC to solidify. 3D PEC templates (10 × 10 × 2 mm), consisting of 6 successive layers of alternating horizontal and vertical filaments, were accordingly fabricated. PEC filament diameter was modulated by adjusting the moving speed of the collecting stage and the feed rate of the PEC ink, where a higher feed rate and a slower stage speed resulted in larger filament diameters, and lower feed rates and faster stage speeds created thinner filaments.[35] For these studies, PEC filaments with diameters of 250−350 μm were printed by using a flow rate of 0.45 mL/h and a stage speed of 30 mm/min.

Upon completion of printing, the Pluronic bath containing the PEC scaffolds was placed inside a −80 °C freezer for 2 min to liquefy the Pluronic. The PEC templates were then extracted from the support bath and rinsed with cold DI water to remove the remaining Pluronic. PEC templates were stored in DI water at 4 °C for further use.

2.4. POC Synthesis and Formation of POC Tubular Networks. POC prepolymer was synthesized as previously described.[38] Briefly, equimolar ratios of citric acid and 1,8-octanediol were added to a glass vial and heated to 160 °C under stirring in a mineral oil bath until a clear molten solution formed. At this point, the temperature was lowered to 140 °C and stirred for another 10 min to form the prepolymer solution. The prepolymer was diluted with an equal volume of 100% ethanol and agitated overnight to create a 50% (v/v) stock solution.

To create the POC tubular networks, a dip-coating procedure was developed in which PEC scaffolds were submerged in varying concentrations of POC for 5 min prior to air drying for 10 min to form a single layer of POC coating. The procedure was repeated to achieve the desired number of coating layers with a designated thickness. After coating, excess POC hanging between PEC filaments was carefully removed. POC-coated PEC scaffolds were then

https://doi.org/10.1021/acsami.4c00716
ACS Appl. Mater. Interfaces 2024, 16, 18522−18533

polymerized at 100 °C for 72 h. After polymerization, approximately 1 mm of the edges of the coated scaffolds were trimmed off with a surgical knife, and then submerged in 3 M KBr under agitation to remove the PEC templates. Successful removal of PEC templates was determined by visual inspection of solution removal through the POC channels by using a vacuum aspirator. After PEC removal, the POC tubular networks were thoroughly washed with DI water to remove excess KBr. The lack of PEC precipitation during the wash step also indicated the complete removal of PEC templates from the channels.

After PEC removal, free-standing POC tubular networks with open channels (100−400 μm in diameter) were characterized for wall thickness by careful examination of the cross sections as well as channel diameter. Images were taken by using a Nikon SMZ 1500 stereomicroscope. At least 3 samples per condition were used for measuring the tube wall thickness, where images of 3 randomly selected regions of interest (ROI) were taken and 4 measurements were obtained from each image, leading to 36 total measurements for each condition (n = 36). A minimum of 2 samples and 18 individual measurements were taken to calculate the mean channel diameter (n = 18).

2.5. Tensile Testing of POC Tubular Networks. As-prepared six-layer POC tubular networks were tested for mechanical properties using an Instron 5965 mechanical testing machine with a 5 kN load cell. Specimens were stretched at a crosshead rate of 1 mm/min until failure, and both the stress and strain were recorded. A total of 5 specimens (n = 5) were included for the measurement. Based on the stress−strain plot, the elastic modulus, ultimate stress, and elongation at the point of ultimate stress were determined.

2.6. Microcomputed Tomography of POC Tubular Networks. To visualize the 3D architecture of POC tubular networks and to ensure complete removal of the PEC template, microcomputed tomography (microCT) was used. POC networks, before and after PEC removal, were imaged using a Bruker Skyscan 1272 CMOS (50 kV, 100 μA, 0.1° rotation step). NRECON software was used to reconstruct the images into a 3D model, and CTVox software was used for volume rendering.

2.7. Creation of Porous POC Tubular Networks. To improve the free diffusion of nutrients through the walls of POC tubular networks, particulate leaching was adopted to create micropores within the POC wall. Pulverized NaCl crystals passed through a 30 μm sieve were added to a POC prepolymer solution at a concentration of 3% (w/v), retaining the integrity of tubular structures while yielding diffusible pores through the wall. It was determined that 8.72% of the POC surface area was occupied by NaCl at this concentration (Figure S4, SI), sufficient to allow nutrient exchange while retaining structural integrity. The solution was then sonicated for 20 min to disperse any aggregated NaCl crystals before being used for coating. To avoid sedimentation of NaCl crystals during the coating procedure, drop-coating was developed and used to coat NaCl/POC onto the PEC templates. Briefly, 50 μL of a homogenized NaCl/POC solution was spread evenly over PEC templates and air-dried for 15 min. To ensure a uniform distribution of NaCl crystals in the POC solution during the coating procedure, the solution was vortexed prior to each coating layer. After 5 repeated coatings and removal of excess solution from PEC templates, the NaCl/POC-coated PEC templates were polymerized at 100 °C for 72 h prior to removal of sacrificial PEC templates in KBr solution as described above. Afterward, NaCl/POC tubular networks were soaked in DI water with continuous agitation to leach out NaCl and then dried in a vacuum oven for 24 h. Scanning electron microscopy (SEM) and energy-dispersive X-ray spectroscopy (EDS) were used to confirm the presence of pores and the complete removal of NaCl. Average pore size and diameter were calculated based on the SEM images using ImageJ software (n = 30).

2.8. COMSOL Simulation. To better understand the diffusion of nutrients across the channel walls with varying porosities, COMSOL Multiphysics (ver. 5.6) was used to simulate fluid flow through the channels and subsequent mass distribution of a diluted solute. A simplified setup was used to represent the scenario of POC tubular networks embedded in a hydrogel matrix, i.e., a rectangle with a width of 200 μm and length of 1200 μm, representing the cross section of a segment of a POC channel, surrounded by another rectangle (320 μm width and 1200 μm length) on each side to represent a portion of surrounding hydrogel. Between the center rectangle and outer rectangles was a 60 μm solid gap resembling the impermeable POC channel wall with evenly distributed 18.9 μm microchannels for the pores in the channel wall. The number of microchannels was determined based on the surface area occupied by NaCl in the 1, 2, 3, and 5% POC-NaCl films (Figure S4E, SI). Perfusion through the channels and nutrient transport through the pores were simulated using the laminar flow and transport of diluted species physics modules of COMSOL. Aqueous solution containing a high glucose concentration (17.5 mM) was used as the model fluid, and the fluid velocity was set to 100 μm/s. The simulation was run for a total of 10 min to map the glucose distribution throughout the surrounding matrix.

2.9. Perfusion and Permeability Testing. To ensure the patency and perfusibility of POC channels, 0.1% (w/v) methylene blue (MB) in DI water was loaded in a 5 mL syringe with a 30G needle and injected carefully through the openings of POC tubular networks at a rate of 0.2 mL/h. Both solid wall and porous wall POC tubular networks were perfused with MB on top of clean glass coverslips. Following perfusion, tubular networks were removed and the coverslips were imaged to observe the permeability of MB through the channel walls.

2.10. Synthesis of GelMA and Cell Encapsulation. GelMA was prepared as previously described.[39] Briefly, 10% (w/v) type A gelatin from porcine skin was dissolved in DI water, and then methacrylic anhydride (0.6 g per gram of gelatin) was added to the solution and stirred until homogeneous. The solution was then centrifuged at 3,500g for 3 min to remove unreacted methacrylic anhydride. The collected supernatant was diluted 3× with DI water and then dialyzed within dialysis bags (MW cutoff: 12 kDa) against DI water at 40−50 °C for 14 days to fully remove unreacted methacrylic anhydride. DI water was refreshed every 24 h. After dialysis, the GelMA solution was lyophilized and stored at 4 °C for further use.

For cell casting, GelMA (7%, w/v) dissolved in complete growth media containing the photoinitiator LAP (0.5%, w/v) was sterilized by passing through a sterile 0.22 μm filter and kept at 37 °C until further use. The human fetal osteoblast cell line, hFOB 1.19, was chosen as a model because of its unique properties. hFOB cells have been transfected with a temperature-sensitive mutant gene of the SV40 large T antigen, resulting in thermally responsive cell proliferation at 34 °C and osteogenic differentiation at 39 °C.[40,41] hFOBs were suspended in sterile GelMA solution at a density of 3×10^6 cells/mL and then 300 μL of solution was cast into 3D printed molds (12 × 12 × 5 mm) with sterilized POC tubular networks (10 min in 70% isopropyl alcohol and 30 min UV irradiation on both sides) or no POC tubular networks serving as controls. Upon cross-linking with UV for 30 s, the cell-encapsulated GelMA blocks were trimmed to expose the POC channels for media infiltration and then gently rinsed 3 times with sterile phosphate buffered saline (PBS) prior to further incubation in growth media at 34 °C. Media was refreshed daily.

2.11. Cell Proliferation and Viability Measurement. To determine cell proliferation within the GelMA samples, the CellTiter-Glo 3D assay was performed on days 0, 1, 4, and 7 following the manufacturer's protocol. CellTiter-Glo 3D is a luminescence-based assay that is designed to penetrate 3D hydrogel scaffolds with highly lytic capabilities to increase accuracy compared to other methods, such as resazurin-based assays or MTT. Briefly, at each time point, cultured samples (n = 3) were harvested and cut into 4 equal pieces to ensure sufficient reagent penetration into the center of the gels. CellTiter-Glo 3D reagent (250 μL) was added to the samples along with 250 μL growth media and shaken vigorously for 5 min prior to an additional 25 min incubation for the luminescent signal to develop. Solution (200 μL) was transferred to 96-well plates in duplicate for luminescence measurement using a Biotek Synergy H1 microplate reader with an integration time of 1 s. Readings on days 1, 4, and 7

https://doi.org/10.1021/acsami.4c00716
ACS Appl. Mater. Interfaces 2024, 16, 18522−18533

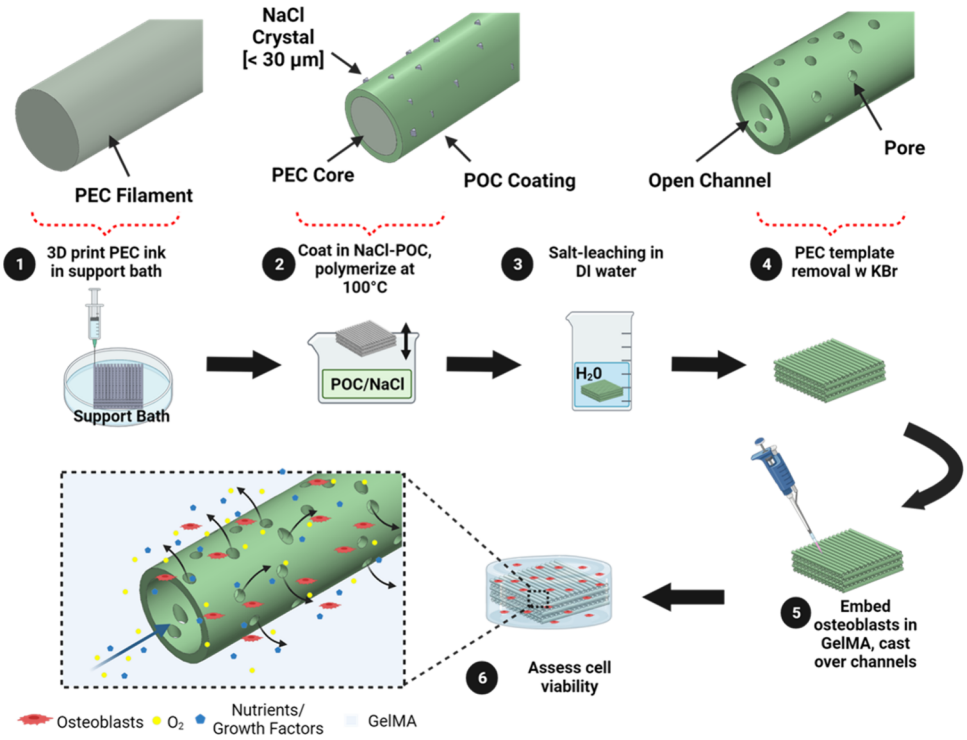

Figure 1. Schematic illustration of the key steps involved in the creation of porous, free-standing tubular networks using 3D printed sacrificial PEC templates and a NaCl-containing POC coating. Images were created with BioRender.

were normalized to their day 0 values to eliminate the variation from the experimental setup; thus, the percent increase in cell number for each condition was calculated.

Cell viability was also analyzed on the 7-day cultured samples using a LIVE/DEAD assay kit. Briefly, samples were rinsed with sterile PBS and then incubated with calcein AM and ethidium homodimer-1 in PBS for 45 min at 37 °C. After being rinsed with PBS, the stained samples were examined by confocal microscopy (Cytation C10, Biotek) and z-stack images were acquired. Live and dead cells were quantified using Gen5 Image Prime 3.11 software (Biotek) and viability was calculated by dividing the number of live cells with the total number of cells (live + dead).

2.12. Fluorescence Staining. After 7-day culture, the cell/GelMA samples were fixed with 4% paraformaldehyde for 2 h at room temperature, permeabilized with 0.1% (w/v) Triton X-100 for 30 min, and blocked for nonspecific binding with blocking buffer (EveryBlot Blocking Buffer, Biorad) for 2 h at room temperature. To visualize the cell morphology, samples were incubated with AlexaFluor 488-conjugated phalloidin (Invitrogen, 1:200 dilution in PBS) for 2 h at room temperature. Images were taken using a Cytation C10 confocal microscope.

2.13. Statistical Analysis. To determine statistical significance, a minimum of three samples were used for each group (n = 3) and results were expressed as mean ± standard deviation. A one-way analysis of variance (ANOVA) and unpaired t test were performed to analyze the data set, and $p < 0.05$ was considered statistically significant.

3. RESULTS AND DISCUSSION

3.1. Fabrication and Characterization of POC Tubular Networks. Following the process as illustrated in Figure 1, free-standing POC tubular networks were fabricated. As a key step toward the fabrication of POC tubular networks, PEC templates composed of six successive layers of filaments were first created from the optimized PDADMAC/PSS coacervate in 1.9 M KBr according to our established embedded printing technique (Figure S1A, SI), as described elsewhere.[35] The PEC filaments of the resultant 3D printed templates were white and opaque (Figures 2B and S1B, SI), while exhibiting a deformed oval shape of the cross section (Figure S1D, SI). We have previously postulated that such an oval shape is most likely caused by the gravity-induced deformation of non-solidified PEC core because of limited water diffusion through the dense and already solidified shell, as shown in the microCT images (Figure S2C, SI). Previously, we did notice that PEC filaments thinner than 120 μm would be fully solidified, having a round transverse shape, whereas those thicker filaments exhibited an oval shape.[35] Close examination of the PEC filaments revealed their relatively smooth surface (Figure S1C,E, SI), which would be favorable to forming a uniform POC coating layer during the dip-coating process.

Theoretically, any material soluble in volatile organic solvents and capable of forming a viscous solution can be used to coat PEC templates. However, in this study, POC was particularly chosen as the coating material due to its extensive utility in vascular engineering[42] and the facile fabrication process of POC prepolymer (fluid phase) and subsequent thermal-induced cross-linking (solid phase). In this study, following the dip-coating process with POC prepolymer, the coated PEC templates were polymerized at 100 °C for 72 h, improving the mechanical properties and decreasing the degree of unreacted monomer available to leach out into solution during subsequent cell studies, thus avoiding acidification of culture media (results not shown).

In the process of coating the POC prepolymer onto the PEC filaments (Figure 2A), establishment of a continuous POC prepolymer layer with desirable thickness would be essential to maintain the patency and structural integrity of the POC tubular networks upon PEC template removal. In this regard, two relevant variables (i.e., POC prepolymer concentration and number of coating layers) were modulated to determine

https://doi.org/10.1021/acsami.4c00716
ACS Appl. Mater. Interfaces 2024, 16, 18522−18533

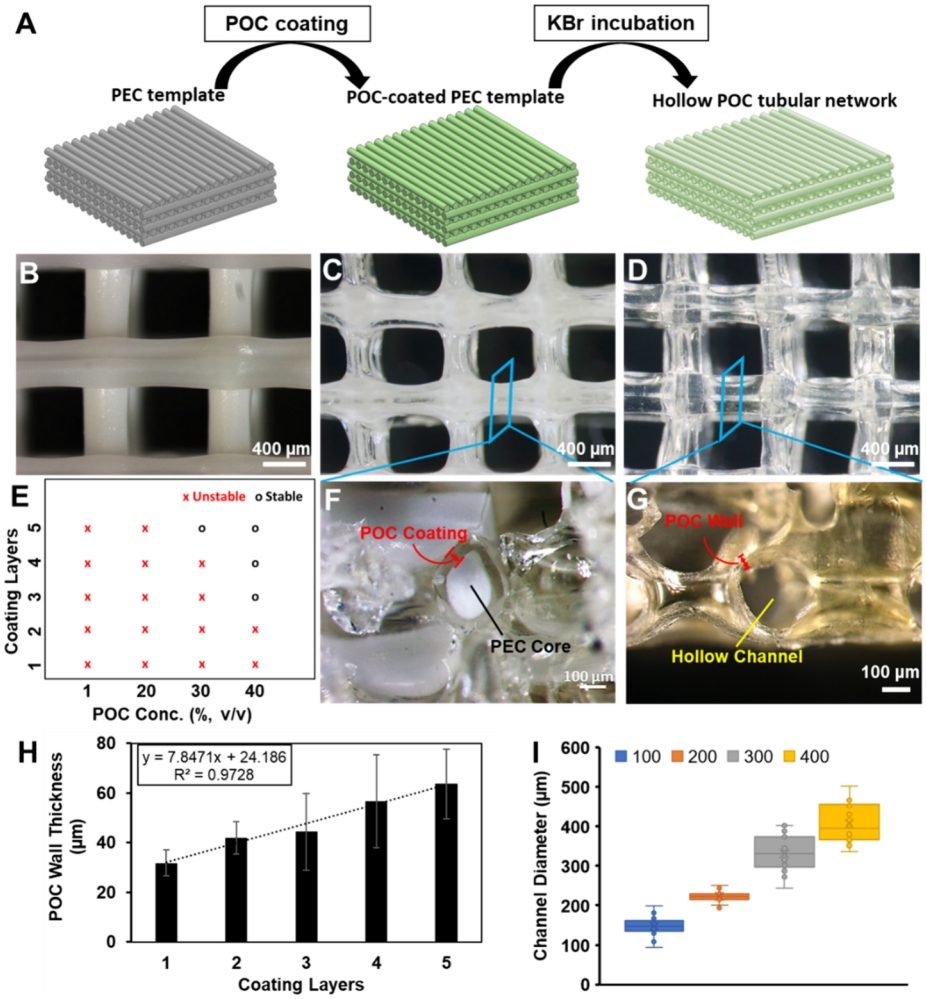

Figure 2. Fabrication of free-standing POC tubular networks. (A) Schematic illustration of the POC coating and subsequent removal of the PEC template core to create POC tubular networks; (B) stereomicroscopic image of 3D printed PEC filaments; (C) stereomicroscopic image of POC-coated PEC templates; (D) stereomicroscopic image of the POC tubular network with hollow channels; (E) graphic depiction of coating layers and POC concentrations suitable to form stable POC channels; (F) stereomicroscopic image of the cross sections of POC-coated PEC filaments; (G) stereomicroscopic image of the cross sections of hollow POC channels after PEC removal with KBr; (H) linear increase of POC wall thickness as a function of the coating layer of POC (n = 36); (I) mean diameters of resultant POC channels deviated from the designed ones using this fabrication process (n = 18).

the optimal coating conditions. It was determined that POC prepolymer concentrations lower than 30% (v/v) were unable to form stable structures after PEC filament removal. While a minimum of 5 coating layers were needed for 30% (v/v) POC prepolymer, increasing the prepolymer concentration to 40% (v/v) required as few as 3 coating layers to form a stable structure (Figure 2E). Considering the difficulty of removing the excess prepolymer from interfilament gaps of PEC templates due to the high viscosity of 50% (v/v) POC prepolymer, this concentration was not further evaluated in this study. To ensure sufficient coating thickness, 40% (v/v) POC prepolymer and 5 coating layers were therefore chosen for subsequent studies.

Upon coating PEC templates with the POC prepolymer and then further thermally cross-linking, the surface of PEC filaments became glossy but remained opaque (Figure 2C) due to the presence of a PEC template core (Figure 2F). Incubation of cross-linked POC-coated PEC templates in 3 M KBr was sufficient to remove the PEC filaments and form hollow lumen structures (Figure 2G). The resultant free-standing POC tubular networks were semitransparent (Figure 2D), consistent with transparency observed with POC films.[38] Examination of the transverse sections of the tubular networks with varying POC layers (up to 5 layers) revealed a linear increase in wall thickness, from 31.8 ± 5.4 (1 layer), 42.0 ± 5.5 (2 layers), 44.4 ± 15.5 (3 layers), 56.7 ± 18.8 μm (4 layers), to 63.7 ± 14.0 μm (5 layers). Each additional layer of POC coating added 8.0 ± 4.3 μm to the wall thickness (Figure 2H). Such a linear increase of wall thickness in relation to the number of coating layers implies the opportunity to further modulate the mechanical properties and dimensions of free-standing tubular networks as needed.

By variation of the embedded printing settings (i.e., PEC feeding rate, printing head moving speed, nozzle size), PEC filament size could be tuned, which subsequently allowed for the modulation of the channel size of POC tubular networks. The minimum and maximum channel diameters were found to be 93 and 502 μm, respectively, and when targeting channel diameters of 100, 200, 300, and 400 μm, the finished channels had the corresponding average diameters of 147.6 ± 23.1, 222.8 ± 14.3, 332.6 ± 43.3, and 414.2 ± 50.0 μm (Figure 2I), suggesting the relative reliability of this approach in creating

https://doi.org/10.1021/acsami.4c00716
ACS Appl. Mater. Interfaces 2024, 16, 18522−18533

tubular networks with desired sizes. These values were within the expected range given previous work using this PEC ink formulation and method for printing.[35] Notably, the resultant POC tubular networks closely followed the shape and architecture of the PEC templates aside from the empty lumen (Figure S2), suggesting the possibility of recapitulating the hierarchical organization of vascular networks by using more complex, biomimicking PEC template designs.

Importantly, the obtained tubular networks retained their structural stability with good handling and manipulation (Figure 3, Video S1, SI), which is critical to maintain the intended patency upon subsequent embedding within a cast material. During physical manipulation, the free-standing POC tubular networks could be easily folded without noticeable damage to the structure and completely recovered their original form in as little as 5 s (Figures 3C vs 3B), confirming the elastomeric nature of POC.[38] Tensile testing was also performed on the as-prepared POC tubular networks, further confirming the elastomeric nature of the scaffolds. The tubular networks exhibited an ultimate stress of 72 ± 17 kPa and elongation of 251 ± 50% at the point of ultimate stress. The average elastic modulus was determined to be 42 ± 12 kPa, demonstrating the elasticity of this material (Figure S4, SI). It was previously observed that successive layers of PEC filaments need to be in contact in order for the printed structure to retain its shape and structural integrity, thus creating points of interconnection between layers.[35] After coating with POC, there is a continuous POC layer connecting the scaffold layers at these intersections (Figure S3B, SI). Close examination of POC tubular networks using microCT reveals hollow junctions at the point of these interconnections, leading to the complete connection of the cross lumens of adjacent layers (Figure S3C,D, SI). Such interconnected lumens would be essential to facilitate the perfusion of media throughout the entire tubular networks.

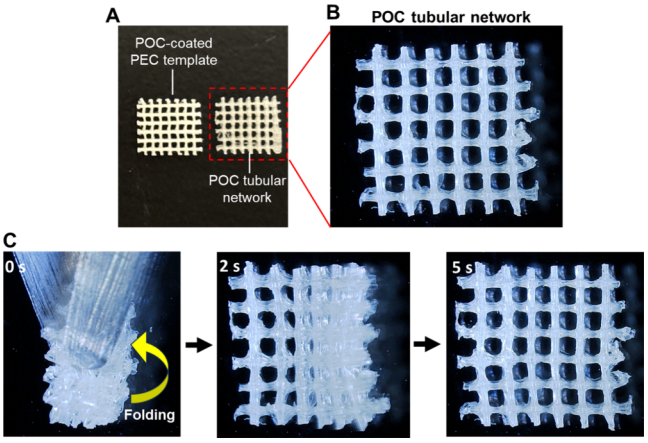

Figure 3. Microscopic images of the free-standing POC microtubular networks before (A, B) and after (C) folding to affirm the structural stability.

3.2. Creation of Micropores through the Walls of POC Tubular Networks. To increase nutrient transport across the tubular walls, i.e., better mimicking the vascular function, salt-leaching was employed to create a microporous structure throughout the POC walls. To avoid the interruption of POC channel structure by larger NaCl crystals, small particulates (<30 μm) were used. Furthermore, the amount of NaCl incorporated in the channel wall may also affect the overall

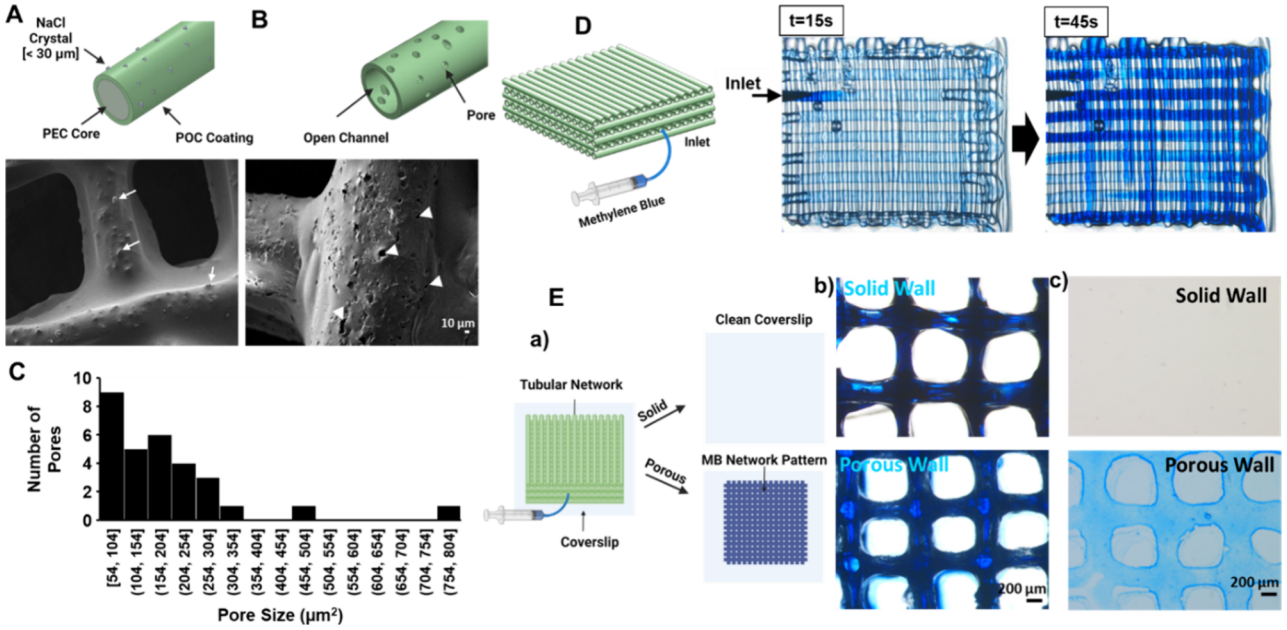

Figure 4. Fabrication and characterization of porous POC tubular networks. NaCl-embedded POC channels before (A) and after (B) salt-leaching to remove NaCl particulates (white arrows indicate salt crystals, and arrow heads indicate pores after salt-leaching). (C) Histogram showing the distribution of pore sizes created after salt-leaching (n = 30). (D) Stereomicroscopic image to show the time-resolved perfusion of 0.1% (w/v) methylene blue solution through the solid wall POC tubular networks. (E) Comparison of the perfusion and diffusion of 0.1% methylene blue solution through the solid wall and porous wall POC tubular networks on the surface of a glass coverslip (a). (b) Stereomicroscopic images of POC tubular networks after perfusion with methylene blue. (c) Stereomicroscopic images of the coverslips after removal of the perfused POC tubular networks, showing a clean coverslip from the solid wall networks and the patterns of methylene blue leaked out of the porous wall networks through the micropores.

https://doi.org/10.1021/acsami.4c00716
ACS Appl. Mater. Interfaces 2024, 16, 18522−18533

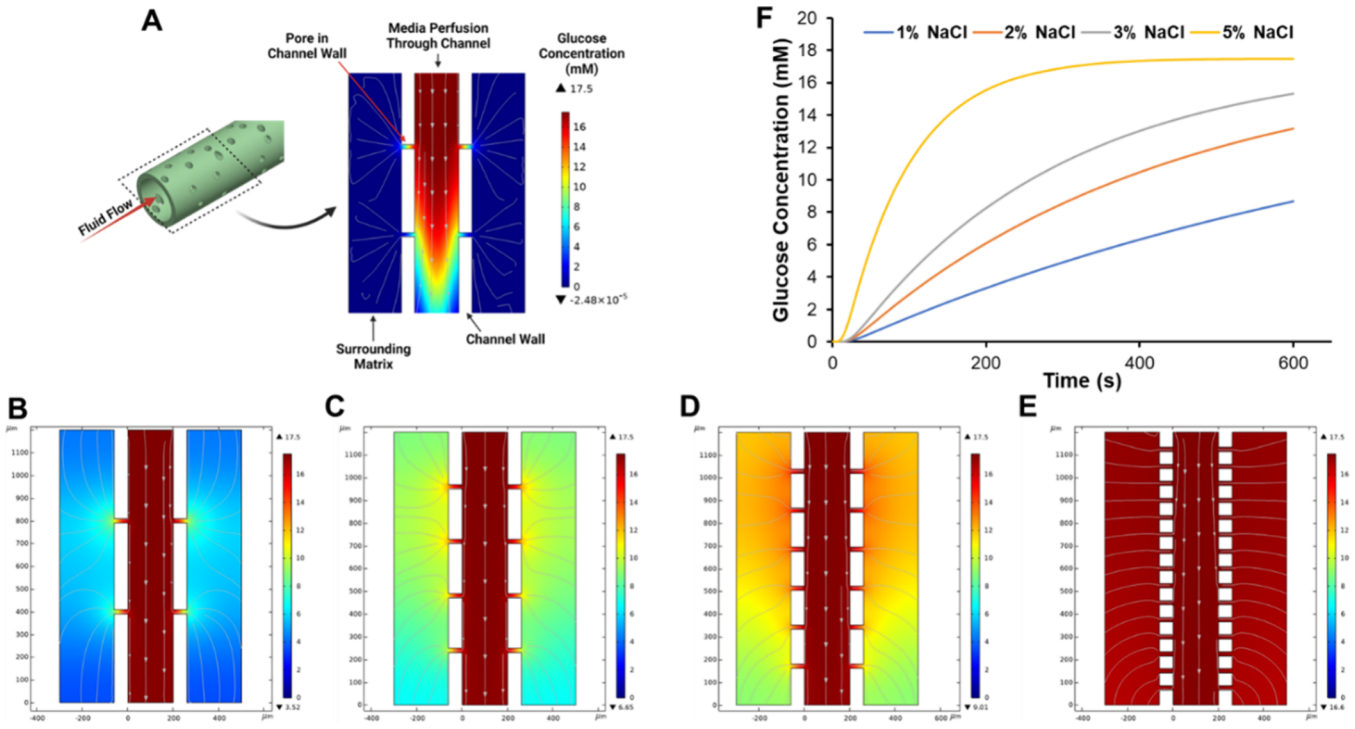

Figure 5. COMSOL multiphysics simulation on the perfusion of media containing 17.5 mM glucose through POC channels with varying porosity. (A) Illustration on the setup of the model with porous POC channel embedded in hydrogel. (B−E) Screenshot images of the simulation on the perfusion of glucose within the POC channel and diffusion out of the channel through the pores of POC walls for 5 min. The POC channel wall has the respective porosity [(B) 1, (C) 2, (D) 3, and (E) 5% (w/v)] based on the concentration of NaCl in the POC solution. (F) Time-resolved concentration change of glucose at 200 μm away from the POC channel wall in the surrounding hydrogel in relation to varying porosity.

channel integrity and the nutrition diffusion capacity. Thus, a POC prepolymer containing different concentrations of NaCl (1−5%, w/v) was cast into films to better determine the correlation between NaCl concentration and the total surface area occupied by NaCl. As anticipated, inclusion of more NaCl in the POC prepolymer led to the proportional increase in the surface area occupied by NaCl, while also showing an increased opportunity to cause NaCl aggregation, particularly with 5% (Figure S5D,E, SI). In this case, 3% NaCl showed better dispersion of NaCl crystals throughout the POC film (Figure S5C, SI), which was consequently adopted for further creation of the microporous POC tubular networks. Examination of the NaCl/POC-coated PEC filaments by SEM revealed the presence of NaCl crystals (bumps) within the otherwise smooth POC surface (Figure 4A). Soaking the NaCl/POC-coated PEC filaments in DI water overnight efficiently leached NaCl out of the POC wall, confirmed by the absence of both sodium and chlorine in the elemental analysis of the pores using EDS (Figure S5, SI). Successful removal of NaCl also led to the formation of micropores across the POC channels. SEM examination of the POC walls revealed abundant, randomly dispersed pores in salt-leached POC channels (Figure 4B). Through ImageJ analysis, it was determined that the median pore size was 163.2 ± 142.4 μm^2 while the average pore diameter was 18.9 ± 5.8 μm (Figure 4C), large enough to transport both small and large molecules through the channel walls[43,44] while also maintaining the structural integrity of the tubular networks. While it has been shown that pores of this size do not promote cellular migration,[45,46] the resultant surface roughness may increase the proliferation and differentiation of various cell types. Fibroblasts seeded on 3D-printed polycaprolactone fibers with micropores created by salt-leaching NaCl crystals less than 30 μm displayed increased proliferation compared to fibers with either larger pores or a smooth surface.[47] In addition, endothelial cells displayed increased cell proliferation on surfaces patterned with micron-sized surface roughness and also showed a higher proliferation and cell alignment on scaffolds with ∼50 μm micro-grooves.[48,49] Pores of this size could be beneficial for endothelial cells to proliferate and migrate along the channel walls and further develop into capillary networks throughout the surrounding matrices upon in vivo implantation. In this regard, to facilitate the angiogenic process, it could also be viable to seed endothelial cells onto the outside of such POC microtubular networks prior to either embedding within cell-encapsulated hydrogels or in vivo implantation. This may serve as an effective strategy toward the fabrication of a fully vascularized scaffold for volumetric tissue engineering, which is highly desirable for reconstructive surgery.[50,51]

3.3. Perfusion and Permeability of POC Tubular Networks. Ideally, the POC tubular networks should allow for continuous perfusion of fluid, such as cell culture media, through the entire interconnected network, while partially diffusing the associated nutrients out of the channels to vitalize the surrounding cells. To demonstrate whether the tubular networks remained patent and interconnected for nutrition to flow through, an aqueous solution containing 0.1% MB, representing the biomolecules, was injected through a single channel inlet of the free-standing tubular network with solid POC walls, as shown in Figure 4D. As noted, the MB solution gradually filled the entire network through the channel layers above and below the initial inlet, evidenced by full perfusion of horizontal and vertical channels (Figure 4D, Video S2, and SI). To our surprise, the MB perfusion did not occur following a

https://doi.org/10.1021/acsami.4c00716
ACS Appl. Mater. Interfaces 2024, 16, 18522−18533

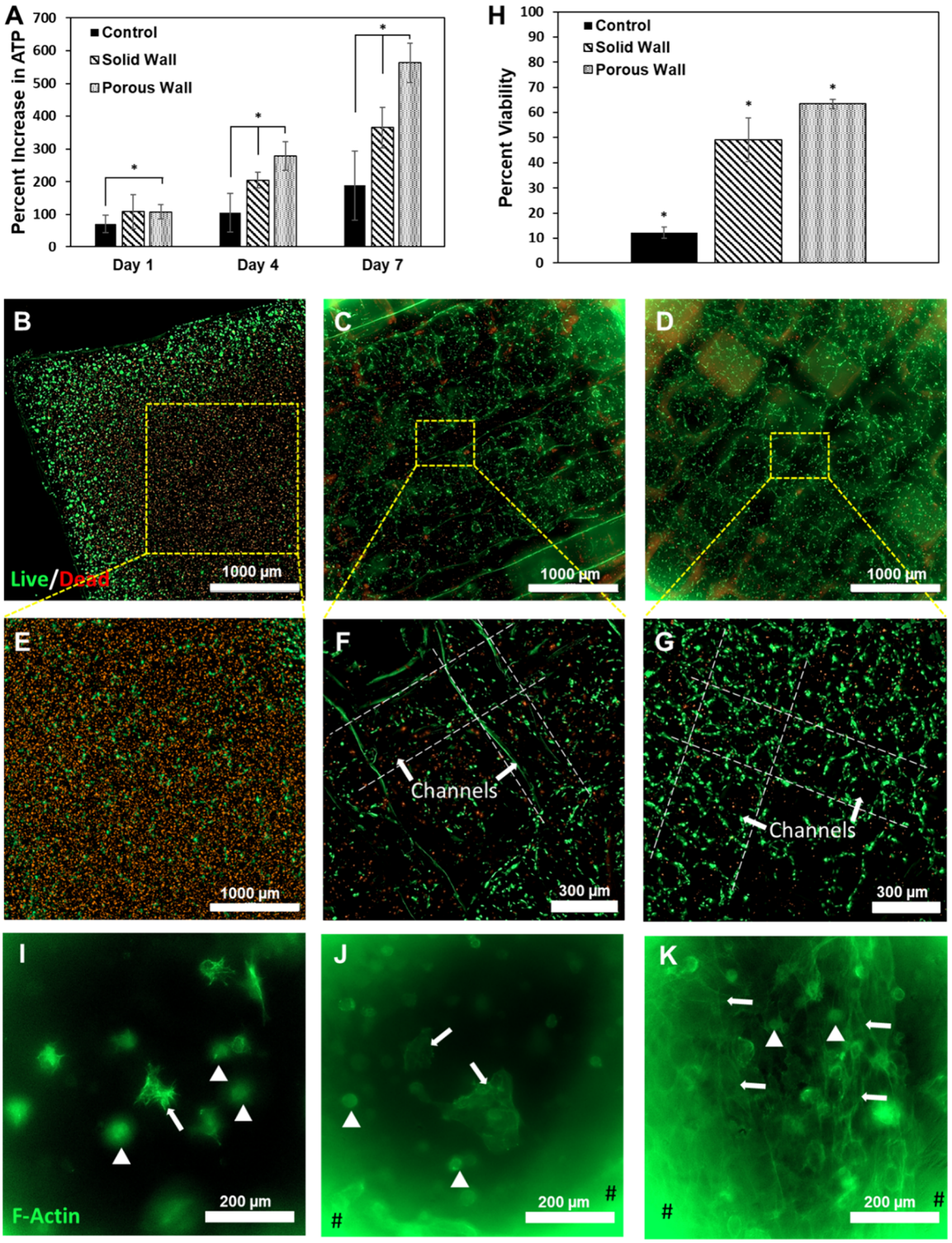

Figure 6. Cell proliferation and viability within the GelMA hydrogel with or without the presence of POC tubular networks (n = 3). (A) Proliferation of hFOB cells within GelMA hydrogel as determined by the CellTiter-Glo 3D assay. The data were normalized by reading on day 0. *p < 0.05. (B−G) Representative fluorescence images of live (green) and dead (red) hFOBs encapsulated in GelMA gel with no channel (B, E), solid wall channel (C, F), or porous wall channel (D, G) after culture for 7 days. The culture was stained with the LIVE/DEAD staining kit. No channel culture shows highly necrotic core (E) with viable cells around the periphery (B). A majority of cells also show a constrained, round morphology with a few of them showing small extensions (I, arrows). Solid wall channels have mostly live cells throughout the scaffold (C) that display a more confined morphology (J), with some dead cells scattered (F, zoom-in image). Porous wall channels have considerably more live cells with a healthy morphology (K) and fewer dead cells than solid wall channels (G, zoom-in image). Dashed white lines indicated channels; scale bars: 1000 (B−E), 300 (F, G), 200 μm (I, J, K). (H) Normalized viable hFOBs encapsulated in GelMA for no channel, solid wall channel, and porous wall channel groups. The quantification was calculated based on live/dead images (n = 5). Fluorescence staining of hFOBs embedded in GelMA without tubular networks (I), solid wall networks (J), and porous wall networks (K) for F-actin (green). Arrowheads indicate round cells, and arrows indicate cells that have spread. Bright green regions indicate autofluorescent POC networks (#). *p < 0.05.

https://doi.org/10.1021/acsami.4c00716
ACS Appl. Mater. Interfaces 2024, 16, 18522−18533

layer-by-layer manner, that is, each individual layer would be perfused and filled with solution before flowing into adjacent layers. Instead, simultaneous infiltration of horizontal and vertical channel layers was observed, which was likely a result of the connected cross-luminal junctions of adjacent layers (Figure S3A,C,D, SI). Differing from the solid wall channels, the introduction of micropores throughout the POC walls should enable the diffusion of nutrients out of the site of perfusion flow and into the surrounding matrix. Such cross-wall diffusion should be closely regulated by the porosity induced through salt leaching.

To better understand the correlation between porosity and nutrient diffusion rate, COMSOL simulations were conducted on a simplified model of porous POC tubular networks (Figure 5A). In these simulations, a 17.5 mM glucose aqueous solution (representing high glucose cell culture media) was perfused at a constant flow velocity of 100 μm/s through the POC channels with porosities corresponding to NaCl/POC ratios of 1, 2, 3, and 5% (w/v). In the simulations, glucose was set to freely diffuse through the micropores of the channel walls into the surrounding hydrogel matrix. Heatmaps generated after 5 min of simulation showed distinct differences in the concentration of glucose diffused into the hydrogel surrounding the channel. At this time point, the highest degree of glucose diffusion was observed with 5% NaCl porosity, reaching 16.6 mM (Figure 5E). In contrast, only 3.52 mM was achieved with 1% NaCl porosity, the lowest among all of the groups (Figure 5B). To benchmark the maximum distance for cells to obtain nutrients from the nearest blood vessel in vivo, the average glucose concentration at 200 μm from the outer edge of the channel wall was measured over the entire 10 min simulation. As shown in Figure 5F, the average glucose concentration increased over time for each porosity group, however, the rate of increase greatly depended on the porosity, with 1% NaCl porosity increasing the slowest and 5% increasing the fastest, as obviously evidenced in the perfusion simulations (Video S3, SI). 1% NaCl porosity was the only group that did not reach 10 mM glucose after 10 min, while 2 and 3% NaCl porosities surpassed 13 and 15 mM, respectively. Interestingly, 5% NaCl porosity displayed a "burst release" of glucose early on and was the only concentration to reach 17.5 mM throughout the simulation. Despite this rapid saturation of glucose observed in the COMSOL simulations, the presence of NaCl aggregates in the 5% NaCl/POC films (Figure S5D) led to the decision to use 3% NaCl for fabricating the porous POC tubular networks.

To validate the COMSOL simulation results and further assess the diffusion capacity of porous POC tubular networks, the MB perfusion study was performed with both solid and porous wall free-standing POC networks on top of clean glass coverslips, as illustrated in Figure 4E(a). Like the solid wall POC networks, porous POC networks were also perfusable with MB (Figure 4E(b)). However, there was observable leakage of MB out of the porous networks onto the glass coverslip during perfusion, leaving behind a pattern identical with the shape of the tubular networks (Figure 4E(c)). This was not observed with the solid wall POC networks, where the coverslip remained clean throughout the perfusion, indicating the increased permeability and leakage caused by the addition of micropores in the POC walls.

3.4. Viability of Cells Embedded in GelMA Hydrogels with the Presence of Porous POC Tubular Networks. To assess the potential for porous POC tubular networks to enhance cell viability in cell-laden volumetric tissue constructs, human fetal osteoblasts (hFOB 1.19) were suspended in 7% (w/v) GelMA hydrogel solution at 3×10^6 cells/mL and cast over sterilized POC networks. This high cell density was chosen to replicate that which is typically required for bone formation, as well as to test the samples in a highly metabolic model.[52−55] Cell-embedded GelMA was cast over the POC tubular networks and then photocrosslinked to form large ($5 \times 5 \times 3$ mm) 3D constructs with dimensions beyond those of oxygen diffusion. The constructs were further cultured for 7 days in static conditions to emulate the circumstances of in vivo implantation. GelMA casts without tubular networks served as controls. Cell proliferation was assessed using the CellTiter-Glo 3D assay, and live/dead staining was used to determine cell viability. As shown in Figure 6A, the presence of tubular networks significantly increased the proliferation of hFOBs encapsulated in GelMA. Notably, the control samples without POC tubular networks showed the lowest cell proliferation by day 7, where only a roughly twofold increase was measured. This is most likely due to the cells within the center of GelMA constructs dying from hypoxia, while only those cells located in the superficial regions were able to obtain the nutrition needed for continued growth. On the other hand, the culture with porous POC tubular networks exhibited the highest cell proliferation for all the time points, reaching 563 ± 60% by day 7. This marked improvement most likely resulted from the elevated transport of nutrients through the micropores of the POC channel walls. Somewhat surprisingly, yet encouragingly, the solid wall POC tubular networks also significantly promoted cell proliferation on day 4 (205 ± 24%) and day 7 (365 ± 62%). Despite the absence of micropores in solid wall POC networks, the thin POC walls might display oxygen permeability and allow for enough oxygen exchange for some cells to proliferate but to a much lesser degree than the porous networks. In addition, the hydrophilic nature of POC might enable the flow of a small volume of media outside of the POC networks at the boundary of the outer edge of the walls and the surrounding GelMA. Further studies would be needed to uncover the underlying causes.

Live/dead staining of 7-day cultured constructs revealed a distinct distribution of live cells among all three groups (Figure 6B−G). Evidently, the constructs without tubular networks had a large necrotic center zone dominated by dead cells, surrounded by peripheral regions rich with live cells. Notably, cells exhibited a considerably smaller and more round morphology, with only a few cells displaying the presence of filopodia (Figure 6I, arrows). Such an observation was consistent with the proliferation assay and agreed with previously reported findings.[56−58] As estimated, the live cell region was about 500 μm in depth from all dimensions, indicating the maximum depth that nutrients and oxygen could reach via simple diffusion. In addition to an appreciable number of dead cells, many live cells also existed in the center of the constructs with solid wall tubular networks. However, these cells did not spread remarkably well, showing a slightly constrained morphology, evident from the fluorescence staining for cytoskeletal protein F-actin filaments (Figure 6J, arrowheads). A small number of cells were able to spread out (Figure 6J, arrows), while a large portion remained round. In contrast, the highest number of live cells with the fewest dead cells was observed throughout the constructs with porous tubular networks, where cells also maintained a highly stretched, healthy morphology (Figure 6K, arrows) and

https://doi.org/10.1021/acsami.4c00716
ACS Appl. Mater. Interfaces 2024, 16, 18522−18533

considerably fewer round cells. Using ImageJ analysis to quantify cell viability, the control, solid wall, and porous wall groups displayed 12 ± 2, 49 ± 9, and 63 ± 2% viability, respectively (Figure 6H). In general, the Live/dead staining results agreed well with the cell proliferation results, indicating the substantial impact on cell viability brought forth by the introduction of micropores.

Surprisingly, despite significant proliferation, there were still a fair number of dead cells present in the constructs with porous tubular networks. These could be attributed to several reasons: (1) potential cell damage caused by the UV irradiation used to cross-link the GelMA, (2) the minimal mass exchange without media perfusion/agitation through the tubular networks may have been enough to support the cells to proliferate, but not enough to maintain the high viability, and (3) the possible release of citric acid from POC degradation may have harmed the cells. It is widely recognized that UV irradiation can cause irreparable DNA damage to cells and the photoinitiators used for GelMA cross-linking could lead to the production of free radicals that further damage cells in the GelMA.[59−61] Although the damage caused by this is often minimal in many cases, further studies should be done to optimize the cross-linking conditions to avoid significant cell death. To mitigate the potential accumulation of citric acid byproducts while also promoting nutrient mass exchange, it would be desirable to culture the 3D constructs containing porous tubular networks in a perfusion bioreactor,[62−64] which is an ongoing effort in our group. Taken together, it is extremely promising that the porous POC tubular networks significantly promoted cell proliferation while maintaining high cell viability over a 7-day period, which is an essential step toward volumetric tissue formation. During this first 7-day period, we would fully expect to see signs of severe necrosis, similar to the control constructs, if prolonged viability would not be supported by the introduction of tubular networks. For this reason, we firmly believe that cells would remain viable for even longer periods of time as long as the tubular networks and GelMA maintain their structural integrity long enough for adequate tissue formation to occur.

4. CONCLUSIONS

In this study, we present a simple yet effective approach to creating porous, free-standing, perfusable tubular networks that can be incorporated in volumetric tissue constructs to improve cell viability. Coating sacrificial PEC filaments with the biocompatible elastomer POC led to the fabrication of mechanically stable, perfusable POC tubular networks upon the facile removal of PEC templates. Furthermore, the inclusion of leachable salt particulates in the POC coating generated micropores through the tubular wall for improved nutrition transfer. Embedding such tubular networks with or without micropores within cell-laden volumetric hydrogel casts significantly improved cell viability compared with those without tubular networks, and the presence of micropores across the channel wall further notably increased cell proliferation and viability. Taken together, this study provides a proof-of-concept for fabricating versatile tubular networks that can be readily incorporated into hydrogel-based tissue-engineered constructs. Alternatively, these tubular networks may serve as 3D scaffolds to support tissue formation to partially address the technical concerns of timely vascularization that have plagued the field of tissue engineering.

ASSOCIATED CONTENT

Supporting Information

The Supporting Information is available free of charge at https://pubs.acs.org/doi/10.1021/acsami.4c00716..

Further nonsentence data and results pertaining to scaffold characterization, COMSOL perfusion simulation videos, methylene blue perfusion video, folding and recovery test video are supplied as Supporting Information of free charge (PDF)

POC network folding (MP4)

POC network perfusion (MP4)

1% NaCl perfusion (MP4)

2% NaCl perfusion (MP4)

3% NaCl perfusion (MP4)

5% NaCl perfusion (MP4)

AUTHOR INFORMATION

Corresponding Author

Hongjun Wang − *Department of Biomedical Engineering and Semcer Center for Healthcare Innovation, Stevens Institute of Technology, Hoboken, New Jersey 07030, United States;* orcid.org/0000-0003-3455-8523; Email: Hongjun.wang@stevens.edu

Authors

Christian Buckley − *Department of Biomedical Engineering and Semcer Center for Healthcare Innovation, Stevens Institute of Technology, Hoboken, New Jersey 07030, United States*

Haoyu Wang − *Department of Biomedical Engineering and Semcer Center for Healthcare Innovation, Stevens Institute of Technology, Hoboken, New Jersey 07030, United States*

Robert O'Dell − *Department of Chemical Engineering, Stevens Institute of Technology, Hoboken, New Jersey 07030, United States*

Matthew Del Rosario − *Department of Biomedical Engineering, Stevens Institute of Technology, Hoboken, New Jersey 07030, United States*

Matangi Parimala Chelvi Ratnamani − *Department of Biomedical Engineering and Semcer Center for Healthcare Innovation, Stevens Institute of Technology, Hoboken, New Jersey 07030, United States*

Mark Rome − *Department of Biomedical Engineering, Stevens Institute of Technology, Hoboken, New Jersey 07030, United States*

Complete contact information is available at: https://pubs.acs.org/10.1021/acsami.4c00716

Notes

The authors declare no competing financial interest.

ACKNOWLEDGMENTS

The authors are thankful for the partial financial support by the National Science Foundation (NSF-GCR award number 2219014) and Army Medical Research and Material Command with award number W81XWH2211044.

REFERENCES

(1) Hoffman, T.; Khademhosseini, A.; Langer, R. Chasing the Paradigm: Clinical Translation of 25 Years of Tissue Engineering. *Tissue Eng. Part A* **2019**, *25* (9−10), 679.

(2) Liu, G.; David, B. T.; Trawczynski, M.; Fessler, R. G. Advances in Pluripotent Stem Cells: History, Mechanisms, Technologies, and Applications. *Stem cell Rev. reports.* **2020**, *16* (1), 3−32.
(3) 2014. doi: Barthes, J.; Özçelik, H.; Hindié, M.; Ndreu-Halili, A.; Hasan, A.; Vrana, N. E. Cell Microenvironment Engineering and Monitoring for Tissue Engineering and Regenerative Medicine: The Recent Advances. *Biomed Res. Int.* **2014**, *2014*, 1.
(4) 2023; Roth, J. G.; Brunel, L. G.; Huang, M. S.; et al. Spatially controlled construction of assembloids using bioprinting. *Nat. Commun.* **2023**, *14* (1), 1−14.
(5) Shafiee, A.; Atala, A. Tissue Engineering: Toward a New Era of Medicine. *Annu. Rev. Med.* **2017**, *68*, 29−40.
(6) Naderi, H.; Matin, M. M.; Bahrami, A. R. Review paper: critical issues in tissue engineering: biomaterials, cell sources, angiogenesis, and drug delivery systems. *J. Biomater Appl.* **2011**, *26* (4), 383−417.
(7) Xie, Z.; Gao, M.; Lobo, A. O.; Webster, T. J. 3D Bioprinting in Tissue Engineering for Medical Applications: The Classic and the Hybrid. *Polymers (Basel).* **2020**, *12* (8), 1717.
(8) Rouwkema, J.; Rivron, N. C.; van Blitterswijk, C. A. Vascularization in tissue engineering. *Trends Biotechnol.* **2008**, *26* (8), 434−441.
(9) Shahin, H.; Elmasry, M.; Steinvall, I.; Söberg, F.; El-Serafi, A. Vascularization is the next challenge for skin tissue engineering as a solution for burn management. *Burn Trauma.* **2020**, *8*, 22.
(10) Zhao, W.; Zhu, J.; Hang, J.; Zeng, W. Biomaterials to promote vascularization in tissue engineering organs and ischemic fibrotic diseases. *MedComm: Biomater. Appl.* **2022**, *1* (1), No. e16.
(11) Song, M.; Zhou, Y.; Liu, Y. VEGF heparinized-decellularized adipose tissue scaffolds enhance tissue engineering vascularization in vitro. *RSC Adv.* **2018**, *8* (59), 33614−33624.
(12) Nuutila, K.; Samandari, M.; Endo, Y.; et al. In vivo printing of growth factor-eluting adhesive scaffolds improves wound healing. *Bioact. Mater.* **2022**, *8*, 296−308.
(13) Jin, K.; Li, B.; Lou, L.; et al. In vivo vascularization of MSC-loaded porous hydroxyapatite constructs coated with VEGF-functionalized collagen/heparin multilayers. *Sci. Rep.* **2016**, *6*, No. 19871.
(14) Laschke, M. W.; Menger, M. D. Vascularization in Tissue Engineering: Angiogenesis versus Inosculation. *Eur. Surg Res.* **2012**, *48* (2), 85−92.
(15) Joshi, A.; Choudhury, S.; Gugulothu, S. B.; Visweswariah, S. S.; Chatterjee, K. Strategies to Promote Vascularization in 3D Printed Tissue Scaffolds: Trends and Challenges. *Biomacromolecules* **2022**, *23* (7), 2730−2751.
(16) Chen, E. P.; Toksoy, Z.; Davis, B. A.; Geibel, J. P. 3D Bioprinting of Vascularized Tissues for in vitro and in vivo Applications. *Front. Bioeng. Biotechnol.* **2021**, *9*, No. 664188.
(17) Gu, J.; Zhang, Q.; Geng, M.; et al. Construction of nanofibrous scaffolds with interconnected perfusable microchannel networks for engineering of vascularized bone tissue. *Bioact. Mater.* **2021**, *6* (10), 3254.
(18) Jia, W.; Gungor-Ozkerim, P. S.; Zhang, Y. S.; et al. Direct 3D bioprinting of perfusable vascular constructs using a blend bioink. *Biomaterials.* **2016**, *106*, 58.
(19) Zhou, X.; Nowicki, M.; Sun, H.; et al. 3D Bioprinting-Tunable Small-Diameter Blood Vessels with Biomimetic Biphasic Cell Layers. *ACS Appl. Mater. Interfaces* **2020**, *12*, 45904−45915.
(20) Bertassoni, L. E.; Cecconi, M.; Manoharan, V.; et al. Hydrogel Bioprinted Microchannel Networks for Vascularization of Tissue Engineering Constructs. *Lab Chip.* **2014**, *14* (13), 2202.
(21) Kinstlinger, I. S.; Saxton, S. H.; Calderon, G. A.; et al. Generation of model tissues with dendritic vascular networks via sacrificial laser-sintered carbohydrate templates. *Nat. Biomed Eng.* **2020**, *4* (9), 916−932.
(22) Chen, X. B.; Fazel Anvari-Yazdi, A.; Duan, X.; et al. Biomaterials/bioinks and extrusion bioprinting. *Bioact. Mater.* **2023**, *28*, 511−536.
(23) Theus, A. S.; Ning, L.; Hwang, B.; et al. Bioprintability: Physiomechanical and Biological Requirements of Materials for 3D Bioprinting Processes. *Polym.* **2020**, *12* (10), 2262.
(24) Xia, Z.; Jin, S.; Ye, K. Tissue and Organ 3D Bioprinting. *SLAS Technol.* **2018**, *23* (4), 301−314.
(25) Ko, Y. G.; Kwon, O. H. Reinforced gelatin-methacrylate hydrogels containing poly(lactic-co-glycolic acid) nanofiber fragments for 3D bioprinting. *J. Ind. Eng. Chem.* **2020**, *89*, 147−155.
(26) Schaefer, N.; Andrade Mier, M. S.; Sonnleitner, D.; et al. Rheological and Biological Impact of Printable PCL-Fibers as Reinforcing Fillers in Cell-Laden Spider-Silk Bio-Inks. *Small Methods.* **2023**, *7* (10), 2201717.
(27) Szymański, T.; Semba, J. A.; Mieloch, A. A.; Cywoniuk, P.; Kempa, M.; Rybka, J. D. Hyaluronic acid and multiwalled carbon nanotubes as bioink additives for cartilage tissue engineering. *Sci. Rep.* **2023**, *13* (1), 646.
(28) Allen, N. B.; Abar, B.; Johnson, L.; Burbano, J.; Danilkowicz, R. M.; Adams, S. B. 3D-bioprinted GelMA-gelatin-hydroxyapatite osteoblast-laden composite hydrogels for bone tissue engineering. *Bioprinting.* **2022**, *26*, No. e00196.
(29) Bendtsen, S. T.; Quinnell, S. P.; Wei, M. Development of a novel alginate-polyvinyl alcohol-hydroxyapatite hydrogel for 3D bioprinting bone tissue engineered scaffolds. *J. Biomed Mater. Res. A* **2017**, *105* (5), 1457−1468.
(30) Gu, J.; Zhang, Q.; Geng, M.; et al. Construction of nanofibrous scaffolds with interconnected perfusable microchannel networks for engineering of vascularized bone tissue. *Bioact. Mater.* **2021**, *6* (10), 3254−3268.
(31) Miller, J. S.; Stevens, K. R.; Yang, M. T.; et al. Rapid casting of patterned vascular networks for perfusable engineered three-dimensional tissues. *Nat. Mater.* **2012**, *11* (9), 768−774.
(32) Eltaher, H. M.; Abukunna, F. E.; Ruiz-Cantu, L.; Stone, Z.; Yang, J.; Dixon, J. E. Human-scale tissues with patterned vascular networks by additive manufacturing of sacrificial sugar-protein composites. *Acta Biomater.* **2020**, *113*, 339−349.
(33) Davoodi, E.; Montazerian, H.; Zhianmanesh, M.; et al. Template-Enabled Biofabrication of Thick 3D Tissues with Patterned Perfusable Macrochannels. *Adv. Healthc. Mater.* **2022**, *11* (7), No. e2102123, DOI: 10.1002/adhm.202102123.
(34) Kolesky, D. B.; Truby, R. L.; Gladman, A. S.; Busbee, T. A.; Homan, K. A.; Lewis, J. A. 3D Bioprinting of Vascularized, Heterogeneous Cell-Laden Tissue Constructs. *Adv. Mater.* **2014**, *26* (19), 3124−3130.
(35) Wang, H.; Zhou, X.; Wang, J.; Zhang, X.; Zhu, M.; Wang, H. Fabrication of channeled scaffolds through polyelectrolyte complex (PEC) printed sacrificial templates for tissue formation. *Bioact Mater.* **2022**, *17*, 261.
(36) Jeong, C. G.; Hollister, S. J. Mechanical, Permeability, and Degradation Properties of 3D Designed Poly(1,8 Octanediol-co-Citrate)(POC) Scaffolds for Soft Tissue Engineering. *J. Biomed. Mater. Res., Part B* **2010**, *93* (1), 141.
(37) Motlagh, D.; Allen, J.; Hoshi, R.; Yang, J.; Lui, K.; Ameer, G. Hemocompatibility evaluation of poly(diol citrate) in vitro for vascular tissue engineering. *J. Biomed. Mater. Res., Part A* **2007**, *82* (4), 907−916.
(38) Yang, J.; Webb, A. R.; Pickerill, S. J.; Hageman, G.; Ameer, G. A. Synthesis and evaluation of poly(diol citrate) biodegradable elastomers. *Biomaterials.* **2006**, *27* (9), 1889−1898.
(39) Loessner, D.; Meinert, C.; Kaemmerer, E.; et al. Functionalization, preparation and use of cell-laden gelatin methacryloyl−based hydrogels as modular tissue culture platforms. *Nat. Protoc* **2016**, *11* (4), 727−746.
(40) Harris, S. A.; Enger, R. J.; Riggs, L. B.; Spelsberg, T. C. Development and characterization of a conditionally immortalized human fetal osteoblastic cell line. *J. Bone Miner. Res.* **1995**, *10* (2), 178−186.
(41) Subramaniam, M.; Jalal, S. M.; Rickard, D. J.; Harris, S. A.; Bolander, M. E.; Spelsberg, T. C. Further characterization of human fetal osteoblastic hFOB 1.19 and hFOB/ERα cells: Bone formation in vivo and karyotype analysis using multicolor fluorescent in situ hybridization. *J. Cell Biochem.* **2002**, *87* (1), 9−15.

(42) Yang, J.; Webb, A. R.; Ameer, G. A. Novel Citric Acid-Based Biodegradable Elastomers for Tissue Engineering. *Adv. Mater.* **2004**, *16* (6), 511−516.
(43) Ling, B.; Oostrom, M.; Tartakovsky, A. M.; Battiato, I. Hydrodynamic dispersion in thin channels with micro-structured porous walls. *Phys. Fluids* **2018**, *30* (7), No. 076601.
(44) Elwinger, F.; Pourmand, P.; Furó, I. Diffusive Transport in Pores. Tortuosity and Molecular Interaction with the Pore Wall. *J. Phys. Chem. C* **2017**, *121* (25), 13757−13764.
(45) Mastrullo, V.; Cathery, W.; Velliou, E.; Madeddu, P.; Campagnolo, P. Angiogenesis in Tissue Engineering: As Nature Intended? *Front. Bioeng. Biotechnol.* **2020**, *8*, 188.
(46) Murphy, C. M.; Haugh, M. G.; O'Brien, F. J. The effect of mean pore size on cell attachment, proliferation and migration in collagen−glycosaminoglycan scaffolds for bone tissue engineering. *Biomaterials.* **2010**, *31* (3), 461−466.
(47) Shabab, T.; Bas, O.; Dargaville, B. L.; Ravichandran, A.; Tran, P. A.; Hutmacher, D. W. Microporous/Macroporous Polycaprolactone Scaffolds for Dental Applications. *Pharmaceutics* **2023**, *15* (5), 1340.
(48) Zhou, K.; Li, Y.; Zhang, L.; et al. Nano-micrometer surface roughness gradients reveal topographical influences on differentiating responses of vascular cells on biodegradable magnesium. *Bioact. Mater.* **2021**, *6* (1), 262−272.
(49) Govindarajan, T.; Shandas, R. Microgrooves Encourage Endothelial Cell Adhesion and Organization on Shape-Memory Polymer Surfaces. *ACS Appl. Bio Mater.* **2019**, *2* (5), 1897−1906.
(50) Kawecki, F.; Galbraith, T.; Clafshenkel, W. P.; Fortin, M.; Auger, F. A.; Fradette, J. In vitro prevascularization of self-assembled human bone-like tissues and preclinical assessment using a rat calvarial bone defect model. *Materials (Basel)* **2021**, *14* (8), 2023.
(51) Anand, M.; Bhagania, M.; Kaur, K. Tissue engineering in plastic and reconstructive surgery: fostering advances in the 21st century via an understanding of the present state of the art and future possibilities. *Arch Aesthetic Plast Surg.* **2023**, *29* (2), 64−75.
(52) Bitar, M.; Brown, R. A.; Salih, V.; Kidane, A. G.; Knowles, J. C.; Nazhat, S. N. Effect of cell density on osteoblastic differentiation and matrix degradation of biomimetic dense collagen scaffolds. *Biomacromolecules* **2008**, *9* (1), 129−135.
(53) Nasello, G.; Alamán-Díez, P.; Schiavi, J.; Pérez, MÁ; McNamara, L.; García-Aznar, J. M. Primary Human Osteoblasts Cultured in a 3D Microenvironment Create a Unique Representative Model of Their Differentiation Into Osteocytes. *Front. Bioeng. Biotechnol.* **2020**, *8*, 336.
(54) Zhang, J.; Wehrle, E.; Adamek, P.; et al. Optimization of mechanical stiffness and cell density of 3D bioprinted cell-laden scaffolds improves extracellular matrix mineralization and cellular organization for bone tissue engineering. *Acta Biomater.* **2020**, *114*, 307−322.
(55) Grayson, W. L.; Bhumiratana, S.; Cannizzaro, C.; et al. Effects of Initial Seeding Density and Fluid Perfusion Rate on Formation of Tissue-Engineered Bone. *Tissue Eng. Part A* **2008**, *14* (11), 1809.
(56) Silva, MMCG; Cyster, L. A.; Barry, J. J. A.; et al. The effect of anisotropic architecture on cell and tissue infiltration into tissue engineering scaffolds. *Biomaterials* **2006**, *27* (35), 5909−5917.
(57) Bertassoni, L. E.; Cecconi, M.; Manoharan, V.; et al. Hydrogel bioprinted microchannel networks for vascularization of tissue engineering constructs. *Lab Chip.* **2014**, *14* (13), 2202−2211.
(58) Suvarnapathaki, S.; Wu, X.; Lantigua, D.; Nguyen, M. A.; Camci-Unal, G. Breathing life into engineered tissues using oxygen-releasing biomaterials. *NPG Asia Mater.* **2019**, *11* (1), 1−18.
(59) Fedorovich, N. E.; Oudshoorn, M. H.; van Geemen, D.; Hennink, W. E.; Alblas, J.; Dhert, W. J. A. The effect of photopolymerization on stem cells embedded in hydrogels. *Biomaterials.* **2009**, *30* (3), 344−353.
(60) Monteiro, N.; Thrivikraman, G.; Athirasala, A.; et al. Photopolymerization of cell-laden gelatin methacryloyl hydrogels using a dental curing light for regenerative dentistry. *Dent Mater.* **2018**, *34* (3), 389−399.
(61) Nguyen, A. K.; Goering, P. L.; Elespuru, R. K.; Das, S. S.; Narayan, R. J. The Photoinitiator Lithium Phenyl (2,4,6-Trimethylbenzoyl) Phosphinate with Exposure to 405 nm Light Is Cytotoxic to Mammalian Cells but Not Mutagenic in Bacterial Reverse Mutation Assays. *Polymers (Basel)* **2020**, *12* (7), 1489.
(62) Ball, O.; Nguyen, B. N. B.; Placone, J. K.; Fisher, J. P. 3D Printed Vascular Networks Enhance Viability in High-Volume Perfusion Bioreactor. *Ann. Biomed Eng.* **2016**, *44* (12), 3435−3445.
(63) Dupard, S. J.; Garcia, A. G.; Bourgine, P. E. Customizable 3D printed perfusion bioreactor for the engineering of stem cell microenvironments. *Front Bioeng Biotechnol.* **2023**, *10*, No. 1081145.
(64) Gabetti, S.; Masante, B.; Cochis, A.; et al. An automated 3D-printed perfusion bioreactor combinable with pulsed electromagnetic field stimulators for bone tissue investigations. *Sci. Rep.* **2022**, *12* (1), No. 13859.

https://doi.org/10.1021/acsami.4c00716
ACS Appl. Mater. Interfaces 2024, 16, 18522−18533